Microflotronics: A Flexible, Transparent, Pressure-Sensitive Microfluidic Film

*Ruya Li, Baoqing Nie, Philip Digiglio, and Tingrui Pan**

There is an increasing demand for sensitive, flexible, and low-cost pressure sensing solutions for health monitoring, wearable sensing, robotic and prosthetic applications. Here, the first flexible and pressure-sensitive microfluidic film is reported, referred to as a microflotronic, with high transparency and seamless integratability with the state-of-the-art microelectronics. The microflotronic film represents the initial effort to utilize a continuous microfluidic layer as the sensing elements for large-area dynamic pressure mapping applications, and meanwhile an ultrahigh sensitivity of 0.45 kPa^{-1} has been achieved in a compact, flexible, and transparent packaging. The response time of the device is in the millisecond range, which is at least an order of magnitude faster than that of its conventional flexible solid-state counterparts. In addition, the fabrication process of the device is fully compatible with the industrial-scale manufacturing of capacitive touchscreen devices and liquid-crystal displays. The overall device packaging can be as thin as 200 μm with an optical transparency greater than 80%. Several practical applications were successfully demonstrated, including surface topology mapping and dynamic blood pressure monitoring. The microflotronic devices offer an alternative approach to the solid-state pressure sensors, by offering an unprecedented sensitivity and ultrafast response time in a completely transparent, flexible and adaptive platform.

1. Introduction

Pressure sensing has acquired extensive interest in both academic and industrial research over the past few years, as the demand for advanced robotics, smart medical prosthetics, and more recently, wearable consumer electronics continues to grow.[1] Flexible substrates and materials have been increasingly utilized in these applications, because of the adaptability and conformability offered to the surfaces with different geometries and topologies. In prior literature, piezoelectric, resistive, capacitive and optical devices have been constructed and demonstrated, with mechanical sensing capacities on a variety of flexible substrates, including elastomeric nanocomposites and primarily deformable polymeric films (e.g., polyimide/PI, polyvinylidene fluoride/PVDF or poly(3,4-ethylenedioxythiophene): poly(styrenesulfonate)/PEDOT:PSS).[2–17] However, the intrinsic properties of these materials impose severe limitations on their potential applications they can be utilized for. For instance, the charge leaking nature of PVDF leads to poor DC response, while the slow recovery and mechanical hysteresis of the resistive nanocomposites have a restricted operating bandwidth less than 5 Hz.[2,6] Moreover, the capacitive sensors with small capacitances are subject to various parasitic capacitances and sources of environmental noise, and optical coupling can present a challenge within any optical pressure sensing design.[13,15]

Recently, microfluidics-enabled sensing devices have shown promise in an array of unconventional applications, such as chemical and biological analyses, cellular manipulations, and electronic skin applications, by providing considerable sensitivity, favorable adaptability, and high flexibility, in which a minute amount of liquid substance responds to an external load by altering its physical properties or geometry.[11,18–26] Microfluidic sensors can employ either detectable changes in optical properties of a miniature flow, or utilize the resistive or capacitive variations in a conductive fluid (e.g., liquid metals and ionic liquids). In general, a low-viscosity working fluid is highly desirable with its physicochemical stability over a broad electrical potential window. Additional material considerations are directly related to the detection principles employed. For resistive sensing, high resistivity of the fluid should be one of the primary selection criteria to achieve high sensitivity, while capacitive sensing should require a fluid with high permittivity for operation. In our previous study we demonstrated that an ultrahigh-capacitive interface forms at an elastic electrolyte-electrode contact can be utilized as a flexible pressure-sensing scheme with substantially improved pressure-to-capacitance sensitivity of 0.43 nF kPa^{-1}.[27]

In this communication, we report the first effort to achieve large-area dynamic pressure mapping by a flexible, transparent, pressure-sensitive microfluidic structure embedded with a continuous thin liquid sensing layer, referred to as microflotronic film (i.e., "microfluidics" + "electronics"), which is well suited

R. Li, B. Nie, P. Digiglio, Prof. T. Pan
Micro-Nano Innovations (MiNI) Laboratory
Department of Biomedical Engineering
the University of California
Davis 95616, USA
E-mail: tingrui@ucdavis.edu

R. Li
Department of Electrical and Computer Engineering
The University of California
Davis 95616, USA

DOI: 10.1002/adfm.201401527

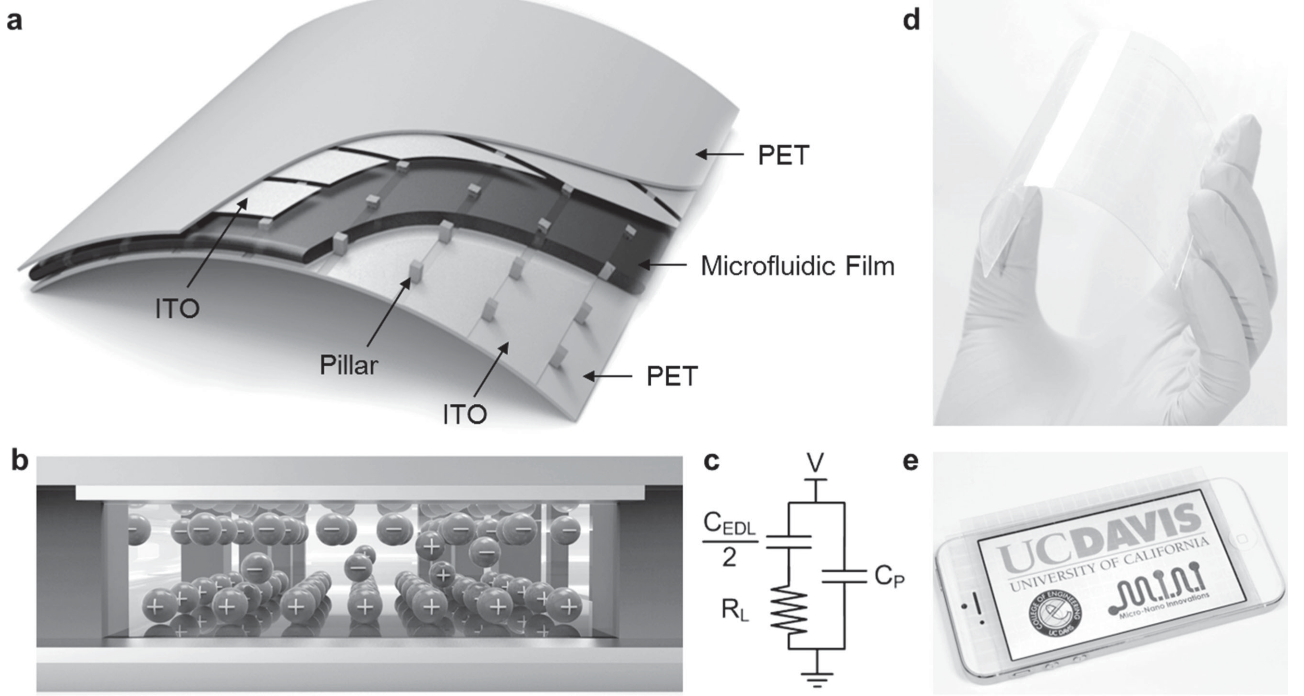

Figure 1. a) Schematic illustration of the microflotronic device structure, consisting of the top and bottom electrode layers with an orthogonally placed electrode array, supported by a micropillar layer and filled with a microfluidic sensing layer. b) Cross-sectional sketch of the device sensing principle: ions in the microfluidic film accumulate at the liquid-electrode contacts which generate the EDL capacitances. c) An EDL capacitance (C_{EDL}) exists at each liquid-electrode contact. The microfluidic film contributes to the liquid resistance (R_L). The overlapped electrode patterns have parallel plate capacitance (C_P). External voltage (V) was applied to the top and bottom electrodes for the measurement. d) Photograph of the microflotronic film 18 by 10 array with a 5×5mm^2 spatial resolution showing flexibility and transparency. e) Photograph of the device placed over the cell phone screen, illustrating the optical transparency of the novel liquid thin-film sensing design.

to pressure and force mapping applications of various surface topologies and geometries. Specifically, the novel impedance-based pressure sensing film consists of flexible top and bottom electrode layers patterned with orthogonally aligned transparent microelectrode arrays, separated by mechanically supporting microstructures, between which is filled with a transparent microfluidic sensing layer. Upon the application of an external load, the force-sensing membranes experience shape deformation, leading to displacement in the microfluidic volume, as well as corresponding changes in the capacitive and resistive values (and therefore, the overall impedance) between the overlapping electrodes. It is desirable for the selected working fluid to possess a certain degree of electrical conductivity to achieve the optimal impedance change and device sensitivity. Utilizing the current matrix design, we have achieved a maximum device sensitivity of 0.45 kPa^{-1} with a center-to-center distance of 5 mm for each sensing unit, which is comparable with the spatial resolution of the mainstream touchscreen technologies.[28] The overall device packaging can be as thin as 200 μm with an optical transparency greater than 80%. In comparison with conventional flexible solid-state counterparts primarily made from conductive composite materials, the fluidic sensing units enable facilitated mechanical responses in the millisecond range, which is at least an order of magnitude faster.[6,29] Moreover, the entire fabrication process of such microfluidic pressure-sensing matrixes is fully compatible with the industrial-scale manufacturing of capacitive touchscreen devices and liquid-crystal displays, which permits scalable production at a significantly lower unit-cost for the lightweight, ultraflexible, large-array sensing devices.[28,30–34] **Figures 1**d–e present photographs of the microflotronic film array (18 by 10) with a 5×5 mm^2 spatial resolution, illustrating the mechanical flexibility and optical transparency of the novel liquid thin-film sensing design to visible light wavelengths.

2. Theoretical Model

Figure 1a illustrates the structural assembly of the microflotronic film array. A microfluidic film fills in the space between two polyethylene terephthalate (PET) films with micropatterned indium-tin-oxide (ITO) coatings. An elastic micropillar array serves as a separation layer between the two deformable membranes. The working fluid is selected to achieve the desired performance, dependent on the optimal device sensitivity and the different length scales. The impedance-based microflotronic sensing principle is demonstrated in Figure 1b. The microfluidic film can be regarded as a resistive element (R_L) in the equivalent circuitry shown in Figure 1c, whereas the device capacitance results from the electrical double layer (EDL) capacitance (C_{EDL}) presented at the liquid-electrode interface and the parallel-plate capacitance (C_P) from the overlapped electrode patterns.[35] When an external load is pressed against the sensing membranes, the microfluidic film between the two electrodes deforms accordingly, leading to detectable changes, primarily in the resistive value at low frequencies (<30 kHz). Because of the dominance of the EDL capacitance, C_{EDL}, the device capacitance experiences only marginal variations under such a structural deformation as the effective interfacial contact areas between the liquid and electrodes remain largely unaffected.

As described previously, the device sensitivity can be derived from the shape deformation of the pressure-sensing film under applied mechanical loads and the corresponding impedance changes of the microfluidic layer between the overlapped electrodes. The mechanical deflection of the sensing membranes can be predicted by using the classic thin plate theory.[36] As a concentrated load (P) is applied onto the center of a square-shaped sensing membrane, the deflection (w) of the membrane is given by the following equation:

$$w = \frac{3}{16}\frac{\left(1-\nu^2\right)\left(a^2-r^2\right)}{Eh^3}\left(\frac{5+\nu}{1+\nu}a^2-r^2\right)P \tag{1}$$

where a and h represent the length and the thickness of the membrane, E and ν indicate Young's modulus and Poisson ratio, respectively, of the membrane construct, and r is the radial distance from the center of the membrane. It is important to note that the size (a) of the membrane, carrying 4th power in the equation, plays the most influential role in determining the membrane deflection. In addition, the membrane deformation has been shown to be inversely proportional to the 3rd power of the membrane thickness, which could be another important factor in the device performance.

In the coupled electrical model, the impedance change of the microfluidic layer can be calculated by using a finite element approach, based on the classic Ohm's law $J = \sigma E$.[37–39] Under the membrane deflection, the microfluidic film will deform correspondingly. The current density (J) passes through each point of the surface of the thin-film layer with a homogeneous electrical conductivity (σ), which can be expressed as

$$J = \sigma\frac{\Delta V}{T-w} \tag{2}$$

where ΔV is for the potential drop across the microfluidic film, and T and w represent the original thickness and displacement of the microfluidic layer, respectively. The total electrical current can be calculated by integrating the current density over each equal potential point, because the fringing effect is insignificant in such a thin-film configuration.[38,40] (See Supporting Information for the detailed mathematical derivations and simulation results.)

3. Results and Discussions

3.1. Fluidic Sensing Materials

As aforementioned, the selection of the working fluid for the intended application is crucial in order to achieve the optimal device performance. Specifically, for a single sensing element of 0.1 × 5 × 5 mm^3, the EDL capacitance is on the order of 100 nF presented at the liquid-electrode interface while the corresponding parallel-plate capacitance stays on the order of 100 pF, which can often be neglected. Of key importance, EDL capacitance only changes by a negligible amount as the membranes deforms. Therefore, the resistive variation in the microfluidic layer becomes the dominant parameter to be detected. Hence, an ideal working fluid needs to satisfy the following criteria: high electrical resistivity, low fluid viscosity, and low vapor pressure over a broad range of operating temperatures. As shown in the theoretical model, the high electrical resistivity leads to an appreciable resistance change caused by the mechanical load despite the presence of parasitic noises, e.g., that from ITO electrodes (in the kΩ range).

The low fluid viscosity permits both rapid mechanical response to external stimuli and low hysteresis, which can be of critical importance to transient and dynamic sensing applications.[41] Moreover, the low vapor pressure ensures the stable conductivity and viscosity without being substantially affected by environmental factors (e.g., humidity level and operating temperature). **Table 1** summarizes the physiochemical properties of several commonly available working fluids for comparison. As shown in the table, deionized (DI) water and ethanol both have relative high vapor pressures at room temperature.[42,43] An imidazolium-based ionic liquid, i.e., 1-ethyl-3-methylimidazolium tricyanomethanide ([EMIM][TCM]), possess relative low viscosity and low vapor pressure, but its high electrical conductivity results in poor sensitivity in our sensor configuration. In contrast, the electrical conductivity of silicone oil is too poor to serve as an electrical sensing medium.[44] Ethylene glycol, propylene glycol, and glycerol all meet the requirements of low electrical conductivity and low vapor pressure.[43,45,46] However, glycerol possesses an extremely high dynamic viscosity at room temperature.[42] Therefore, ethylene glycol (EG) is selected as a suitable working fluid as it offers the desired combination of all of the properties described above, including low viscosity to achieve optimal transient and rapid response characteristics. Although EG has low vapor pressure, hermetic packaging would further reduce evaporation rate, but requires a different fabrication process and construct materials, which may not allow us to achieve all the features presented in this study. On the other hand, adding permeation barrier layer (e.g., SiO_x and SiN_x) on the substrates can further reduce the evaporation.[47]

Table 1. Comparison of physical and chemical properties of some commonly available fluids

	Electrical Conductivity [S m^{-1}]	Viscosity[b] [mPa s]	Vapor Pressure[c] [kPa]
Ethylene Glycol	1.07×10^{-4}	16	0.0075
Propylene Glycol	1×10^{-5}	40.4	0.017
Glycerol	4.25×10^{-6}	934	<0.00033
DI water	5.5×10^{-6}	0.89	2.3
Ethanol	N/A	1.203	5.83
Silicone Oil[a]	$\approx 10^{-13}$	1–2000	0.667
Ionic Liquid ([EMIM][TCM])	1.8	18	N/A

[a] Property differs for various silicone oil blends; [b] At 25 °C; [c] At 20 °C.

3.2. Characterization of Device Sensitivity

As mentioned in the theoretical analysis, geometrical design can play a considerable role in determining sensing performance. **Figure 2**a–c shows the characterization results of the device sensitivity with different geometrical parameters, including membrane thickness, spatial resolution, and microfluidic layer height. Specifically, the device sensitivity is evaluated as the relative resistance change (R/R_0) over the centralized pressure load (P). With this method, the sensitivity can be compared directly across samples with different dimensions or length scales. Figure 2a–c summarizes both the experimental measurements and the theoretical analyses for the EG-filled microflotronic device, in which geometrical design has a considerable influence on the device performance. With a sensing membrane thickness of 125 µm and a microfluidic layer height of 100µm, the device sensitivity increases nearly 80 fold from 8.4×10^{-5} kPa^{-1} to 1.3×10^{-3} kPa^{-1} to 6.5×10^{-3} kPa^{-1} as the device spatial resolution increases from 1mm to 2 mm to 3 mm. Furthermore, as indicated in Equation (1), the membrane thickness has a dominant role in determining the sensing performance. In the design utilizing a spatial resolution of 5 mm and a microfluidic layer height of 100 µm, the sensitivities for 175 µm, 125 µm and 75 µm sensing membranes are 0.019 kPa^{-1}, 0.048 kPa^{-1} and 0.18 kPa^{-1}, respectively. These results have illustrated a close agreement with the theoretical prediction, which states that the membrane displacement is correlated with the 3rd power of the membrane thickness. In addition, the microfluidic film thickness determines the initial resistance of the sensing layer, which would affect the overall sensitivity evaluated as the relative resistance change, as well as the corresponding pressure dynamic range. The sensor design with a membrane thickness of 75 µm, a fluidic layer height of 50 µm and a lateral dimension of 5 mm has achieved the highest sensitivity of 0.45 kPa^{-1}, but exhibited the smallest dynamic range of 0 to 1kPa. Another implementation, utilizing a sensing microfluidic layer height of 200 µm, can extend the dynamic pressure range to 4.2 kPa, while reducing the device sensitivity to 0.062 kPa^{-1}. In summary, by adjusting the three key dimensional parameters, that is, the spatial resolution, the membrane thickness and

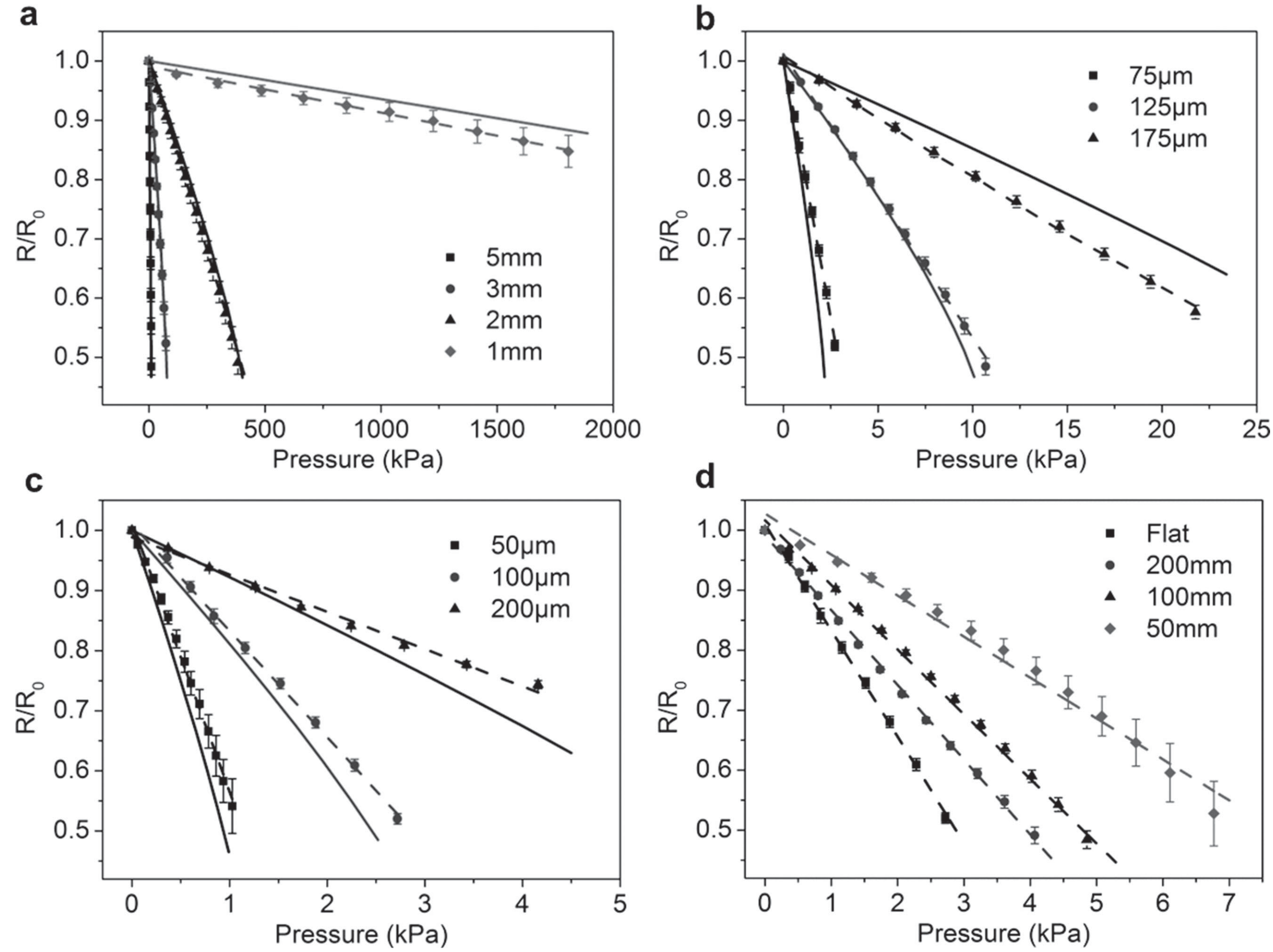

Figure 2. a–c) Plots of the experimental and theoretical microflotronic device sensitivity. The measurement results are plotted as dots with associated error bars and the fitted curves shown with dashed lines, while sensitivity predicted by the theoretical model is shown with solid lines. a) Sensitivity vs the spatial resolution, changing from 1 mm, 2 mm, 3 mm to 5 mm. b) Sensitivity vs the membrane thickness, changing from 75 µm, 125 µm to 175 µm. c) Sensitivity vs the film thickness, changing from 50 µm, 100 µm to 200 µm. d) Device sensitivity under different radii of curvature, changing from 50 mm, 100 mm, 200 mm to infinite (flat). Fitted curves are shown with dashed lines.

the microfluidic film thickness, different device sensitivities (in the range of 8.4 × 10^{-5} kPa^{-1} to 0.45 kPa^{-1}) and various pressure dynamic ranges (in the range of 1 kPa to 1800 kPa) can be achieved and adapted to custom applications.

3.3. Characterization of Bending Effect

To investigate the device performance under bending, we characterized the device sensitivity while it was structurally deformed on the surfaces with different radii of curvature. The microflotronic film was mechanically bent outward along with the direction of the parallel electrode on one side of the sensing membrane. Figure 2d summarizes the relative resistance R/R_0 under different mechanical loads while bent on the surfaces with radii of curvature of 50 mm, 100 mm, 200 mm and infinite (flat), in which the microflotronic devices have a membrane thickness of 75 µm, a fluidic layer height of 100 µm and a spatial resolution of 5 mm. It has been observed that as the radius of curvature of the bent membrane is reduced from 200 mm, 100 mm to 50 mm, the device sensitivity also declines gradually from 0.12 kPa^{-1} , 0.11 kPa^{-1}, to 0.07 kPa^{-1} , given the sensitivity on the flat surface is 0.18 kPa^{-1}. These results have demonstrated that the microflotronic device can be utilized for flexible and curved surfaces, in which additional calibration may be required.

3.4. Response Time and Cyclic Test

As one of its key advantages, microflotronic film exhibits a more rapid mechanical response in comparison with its flexible solid-state counterparts. Time-resolved experiments have been conducted to demonstrate such a facilitated mechanical response. A pulsed pressure load was applied to the device by a piezoelectric actuator (driven by a square-wave signal at 10 V peak-to-peak), and the electrical output was recorded. The working fluids, DI water and EG, with different fluid viscosities were filled into the sensing layer. All of the calibrated sensors share an identical microfluidic layer height of 100 µm, a membrane thickness of 75 µm, and a lateral dimension of 5 mm. **Figure 3**a, 3b and 3c summarizes the mechanical responses of DI water-filled and EG-filled devices to 1Hz, 10Hz and 100 Hz mechanical stimuli. As it can be seen, both microflotronic devices have achieved relaxation time in the millisecond range, while the DI water-filled device reaches a faster response than that of the EG-filled device due to its lower dynamic viscosity (shown in Table 1). These results verify the importance of the fluid viscosity in determining the dynamic response of the device. In comparison, its flexible solid-state counterparts utilizing pressure sensitive rubbers or conductive foams suffer hysteresis caused by the viscoelasticity of the material, which limits their response time to the order of tens to hundreds of milliseconds.[6,29] In conclusion, the rapid mechanical response of the microflotronic device can be facilitated by utilizing a low viscosity liquid as the working fluid. The same testing setup has been also used to evaluate the repeatability of the microflotronic film by applying a cyclic mechanical load with 10 000 cycles. The relative resistance, R/R_0 has been measured and plotted against the number of loading cycles in Figure 3d. As can be seen, the relative resistance change of the device has been assessed with less than 2% in variation after 10 000 testing cycles, illustrating the mechanical repeatability and reliability of the device.

3.5. Characterization of Frequency Dependence

For the dynamic and transient responses, the frequency response becomes an important consideration. To investigate the frequency dependence of the microflotronic device, a LCR meter (4284A, Agilent) was used to measure the reactance (*X*) and resistance (R) in the sub-MHz frequency range. The microflotronic sensing arrays (3 by 3) with either DI water-filled or EG-filled were connected to the LCR meter in a bipolar configuration at 1V AC excitation. Both devices shared a microfluidic layer height of 100 µm, a membrane thickness of 125 µm, and a spatial resolution of 5 × 5 mm^2. Figure 3e plots the frequency (*f*) dependency measurements of the resistance (R) and the reactance (*X*) of the individual device. As shown in Figure 3e, the reactance value of the EG-filled device experiences a decline from 19.3 kΩ at 20 Hz to a minimum value of 0.52 kΩ at 2 kHz, and then rises to 6.1 kΩ at 150 kHz, followed by another decrease to 2.1 kΩ at 700 kHz, whereas the resistive value remains fairly constant between 100 Hz to 30 kHz. Whereas, for the DI water-filled device, the reactance starts to decline at a lower frequency (13.9 kΩ at 20 Hz) until a minimal value of 0.82 kΩ has been reached at 1.5 kHz, then it increases to a peak value of 7.2 kΩ at 70 kHz, and finally drops again to 1.2 kΩ at 200 kHz, while the resistive value remains fairly constant between 100 Hz to 20 kHz. According to our observation, the variation of the device resistance and reactance over the operation frequency range can be predicted based on the device's equivalent circuit. (Detailed frequency dependency theoretical analysis is given in Supporting Information.) Therefore, the optimal operational frequency range is 300 Hz to 30 kHz under the current sensor configuration, while the capacitive reactance remains a minimal constant value.

3.6. Surface Topology Mapping

To demonstrate the potential of the microflotronic array to spatially resolve a pressure distribution and its adaptability to the state-of-the-art electronics, we fabricated an 18 by 10 pixel array with a total surface area of 9 × 5 cm^2, consistent with the area of touchscreens utilized in mainstream smartphones (e.g., iPhone 5/5s). A 100 µm fluid sensing film that monitored the pressure distribution was encapsulated by two 125 µm-thick PET/ITO sensing membranes. The optical transmission of the entire device was measured at 81.8% within the visible light spectrum (The transmittance measurement can be found in the Supporting Information). Further improvement of the optical transmission can be achieved by utilizing electrode surfaces with superior optical transparency.[48] **Figure 4**a–b showed the pressure resolution results of a letter-shaped polymeric stamp placed on top of the microflotronic film. By introducing additional mechanical weight onto the stamp, the

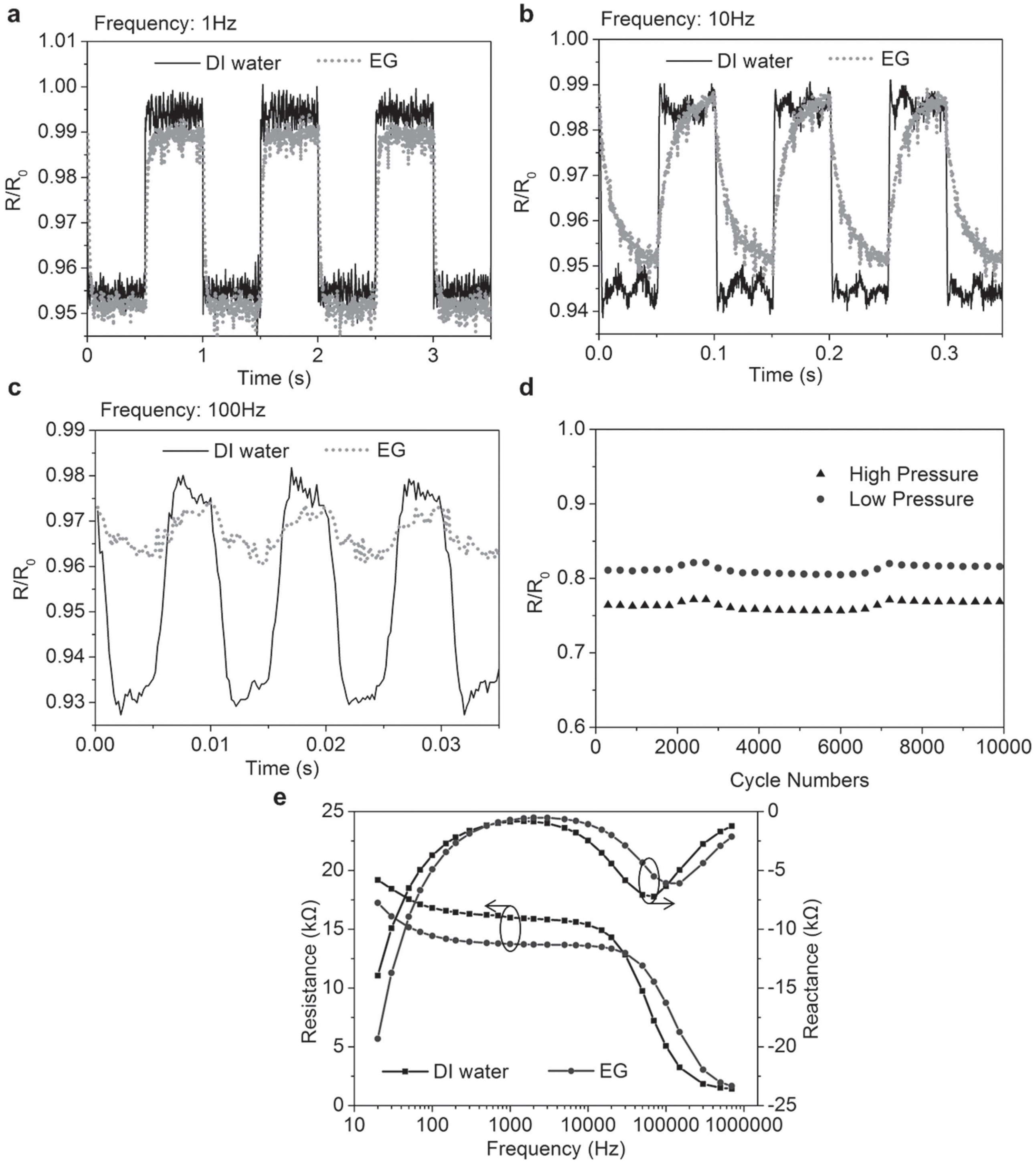

Figure 3. Mechanical response of a microflotronic pressure sensing unit with a microfluidic layer height of 100 μm under varying periodic stimuli of a) 1 Hz, b) 10 Hz, and c) 100 Hz. The blue line represents the output reading from a DI water-filled device; while the red line represents for the output measurement from an EG-filled device. d) Relative resistance as a function of the external pressure cycles, demonstrating the mechanical robustness and stability of the devices after 10,000 cycles of pressure and release. e) Frequency dependence of the device equivalent resistance and reactance.

pressure distribution of the sensing array can be read out in real-time by scanning the impedance values of each single element with the associated interfacial circuitry (see Supporting Information for detailed circuit acquisition). To further explore the potential of the microflotronic devices for 3D touchscreen applications, we dynamically measured the finger pressures applied to the microflotronic film. The mapping result depicted in Figure 4d successfully resolved the position of the finger and

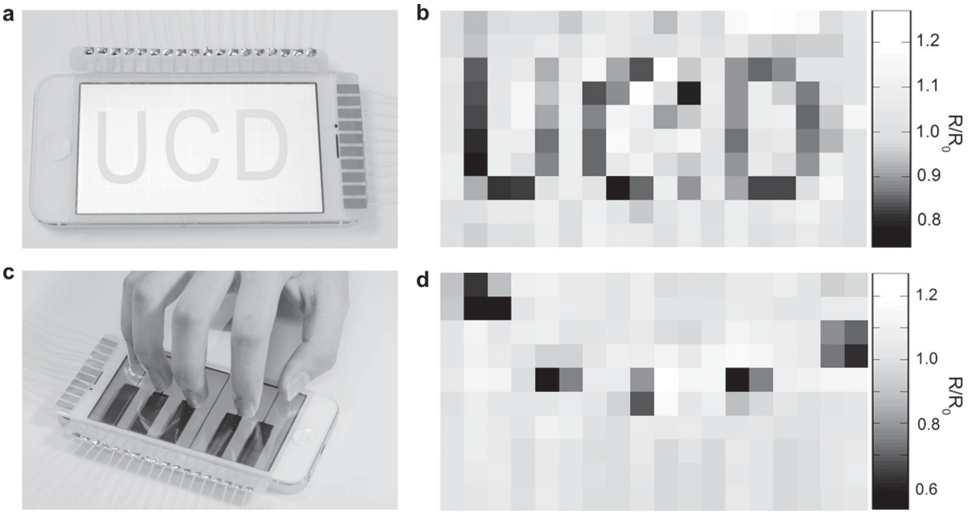

Figure 4. Pressure mapping illustration and results for a–b) polymeric stamps and c–d) finger pressure distribution over a piano app, enabled by an integratable 18 × 10 microflotronic array on a smartphone touchscreen.

the corresponding pressure applied in a real-time mapping. Crosstalk between adjacent elements has been observed, which may be alleviated by further fluid dynamic modelling.[49] The variability in the measurement could attribute to the electrical noise of the readout circuitry and the crosstalk between adjacent sensing elements. This demo of the microflotronic array illustrated the ability of collecting pressure distributions from multiple contacts as well as the overall contact force, which can be calculated by integrating the pressure value measured over each individual element for human-computer interface applications. Unlike regular touchscreens which only detect two-dimensional finger position, the microflotronic array also measured the physical force exerted onto the screen and translated into additional third dimension controls to the computer interface.

3.7. Radial Arterial Pressure Mapping

To demonstrate the microflotronic device's potential for wearable health sensing, the flexible microflotronic sensor was employed to continuously measure the radial arterial pulse utilizing the measurement principle of tonometry. Although a few recent reports showed the potential application of various types of pressure sensors to radial arterial pulse monitoring,[10,50] the proposed microflotronic film array offered not only real-time and continuous recording of the pressure pulse waveform, but the automatic pulse tracking strategy that the optimal positions for pulse recording can be resolved by analyzing the dynamic pressure distribution over the skin surface as shown in **Figure 5**a-c, from which the cumbersome procedure to locate the radial artery can be eliminated for the practical utility in wearable health monitoring. The device employed was a 3 by 3 array with a 5 × 5 mm^2 spatial resolution with a 100 µm fluid film layer encapsulated by two 75 µm thick PET/ITO sensing membranes. Aligning the device on the wrist along the radial artery (Figure 5d), the pressure variation under the 3 by 3 microflotronic array during one cardiovascular cycle was mapped and fitted into continuous pressure distribution surface using spline interpolation as presented in Figures 5a-c. Through the mapping result, the optimal pulse tracking positions were determined based on the maximum pressure variations have been measured. As shown in Figures 5c and 5e, the radial arterial pressure waveforms (P_1 and P_2) represent the largest pressure variations among all the sensing elements of the microflotronic array. The start time was fixed at the end-diastolic pressure in the previous cycle. Peak systolic pressure occurred at time $t_1 = 0.115$s, followed by the dicrotic notch at time $t_2 = 0.337$s and diastolic runoff at time $t_3 = 0.559$s. The radial arterial pressure waveform was clearly resolved by the microflotronic sensor, and all of the key features of the waveform were readily recognized, including the systolic upstroke, the systolic peak pressure, the systolic decline, the dicrotic notch, the diastolic runoff, and the end-diastolic pressure.[51] A key advantage of acquiring the complete pressure waveform continuously is that many pertinent hemodynamic parameters can be directly calculated or estimated in real time such as arterial indexes, upstroke time, stroke volume variation, and even cardiac output.[52,53] Furthermore, as the radial arterial pressure signal was recorded simultaneously from sequential sensing units, another important parameter that can measure arterial stiffness and adverse hemodynamic effects, pulse wave velocity, can be measured by calculating the wave propagation time delay between fixed-spatial-resolution sensing units.[54] By providing the dynamic pressure mapping result with ultrahigh sensitivity, the wearable microflotronic device demonstrated its potential to automatically locate and resolve the arterial pulse waveforms with the delicate pressure events detected non-invasively.

4. Conclusion

A flexible, transparent, pressure-sensitive film has been reported utilizing an embedded microfluidic sensing layer to achieve pressure and force mapping over various surface

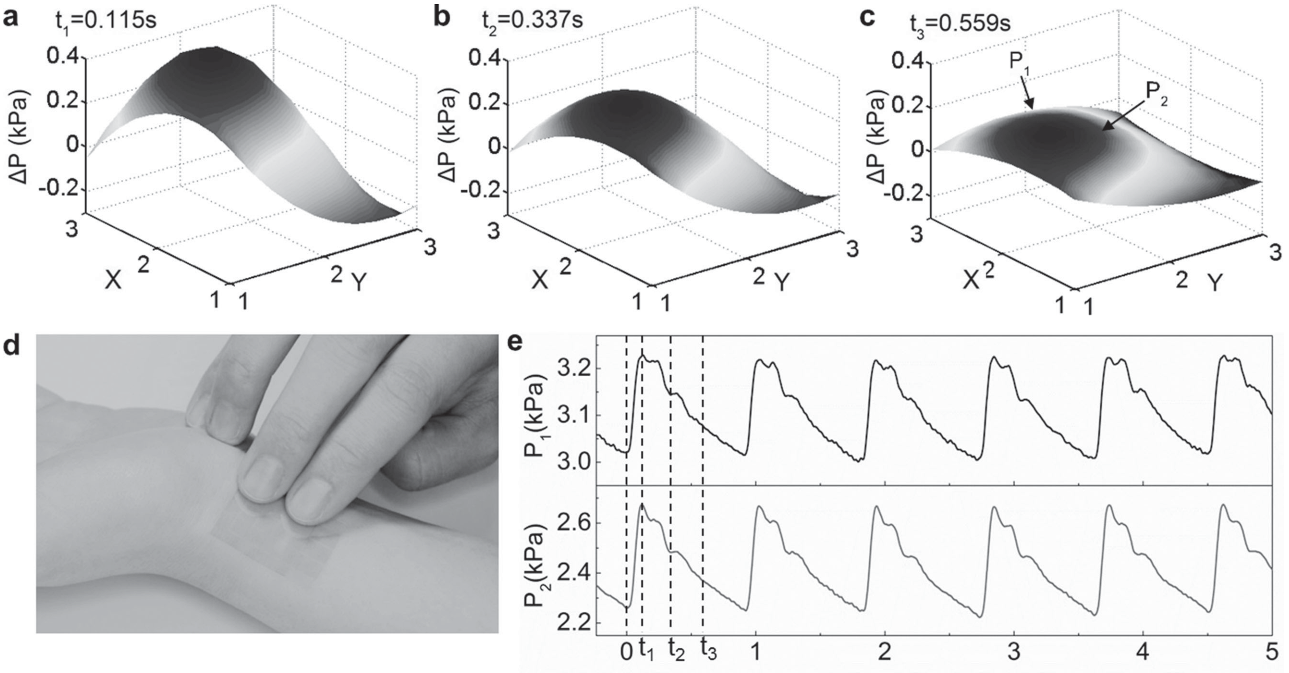

Figure 5. Non-invasive radial artery pressure mapping. Pressure variation mapped by a 3 by 3 microflotronic array during one cardiovascular vascular cycle a) at t_1 = 0.115s, b) at t_1 = 0.337s and c) at t_1 = 0.559s. With the previous end-diastolic pressure fixed at t = 0, pressure variation at a) systolic pressure (at t_1), b) dicrotic notch (at t_2), c) diastolic runoff (at t_3). e) Two continuous pulse pressure signals recorded by two of the nine sensing units. d) Photograph of the 3 × 3 microflotronic array with a spatial resolution of 5 × 5 mm^2 attached to the wrist.

topologies. The novel pressure-sensitive microfluidic film has demonstrated sensitivity up to 0.45 kPa^{-1} in a 200 µm-thick package. As an alternative to the flexible solid-state pressure-sensitive elastomers, the high sensitivity, high transparency, and low-viscosity microflotronic device can offer rapid mechanical responses in a few milliseconds. Moreover, the entire fabrication process of the microflotronic pressure-sensing matrixes is compatible with the industrial-scale production of capacitive touchscreen devices and liquid-crystal displays, which makes scalable manufacturing at low cost feasible in the foreseeable future. In summary, this novel microflotronic film offers a new flexible sensing interface that can be highly advantageous for emerging medical and electronic applications, such as health monitoring, medical prosthesis, 3D touchscreens, and human-machine interfaces, where device sensitivity, surface adaptability, and large-area mapping are all essential.

5. Experimental Section

Microfabrication Process: The device fabrication consisted of four processes, including electrode patterning, spacing layer construction, bonding and microfluidic loading. We patterned the ITO electrodes on PET film (Mianyang Prochema Commercial Co.) using a standard photolithography process, including the use of a dry film photoresist (Alpho NIT215, Japan) and a wet etching process. The designed electrodes had line-line spacing of 500 µm for 5 mm and 3 mm resolution, 250 µm for 2 mm and 1 mm resolution configuration. When constructing the spacing layer, a negative photoresist (PerMX3050, DuPont) was laminated on the ITO patterned PET substrate at 65 °C. After a soft bake at 115 °C for 5 minutes, the substrate was exposed to UV light under a mask aligner (ABM, Inc.) forming the spacing pillar structure between the electrodes. Then, the substrate was post baked under 95 °C for 2 minutes and developed with propylene glycol monomethyl ether acetate (PGMEA>99.5%, Sigma-Aldrich). In order to bond the top layer electrode with the micropillar structured substrate, a layer of PDMS oligomers needed to be transferred onto the bonding area.[55] To transfer the PDMS oligomers, both the top layer electrode and the micropillar structured substrate were activated in an oxygen plasma generator (FEMTO, Diener) at 30 W for 30 seconds. After the activation, the bonding area was contacted with a PDMS stamp for two hours, of which the ratio of the base to the curing agent was set at 15:1. PDMS oligomers deposited on the bonding area can bond to a PDMS film after oxygen plasma treatment at 90 W for 10 seconds. The bonding PDMS film was designed to bond and seal the two ITO/PET films but leaving two microfluidic inlet/outlet ports to be filled with the sensing layer afterwards. Following the liquid loading process, the two ports were completely sealed by PDMS to prevent evaporation. Then curing can be achieved by either setting at room temperature for 24 hours or baking at 80 °C for 2 hours.

Device Characterization Setup: Device sensitivity characterization was conducted on the center unit the 3 by 3 array configuration. Each set of parameters was tested among three identical samples and each sample was measured three times. A force gauge with 0.1 mN resolution (M7-012, Mark-10) was mounted on a computer-controlled step motor (VT-80, PImicos) with 400 nm spatial resolution. The concentrated load was applied and monitored on the sensor as the corresponding impedance change was recorded by an LCR meter (4284 A, Agilent). The pressure values were calculated based on the force readout from the force gauge and membrane area. Mechanical response characterization of the device was conducted by driving a piezoelectric actuator (T215-A4-303 (Y), PIEZO SYSTEMS, INC.) with a 10 V peak-to-peak square wave to apply a periodic contact pressure to the surface of the sensor. The output signal was measured by the readout circuit in a sampling frequency of 250 kHz. Optical transmission was characterized on an 18 by 10 array using a Safire2 plate reader. The reported value of transmission was taken at 550 nm.

Supporting Information

Supporting Information is available from the Wiley Online Library or from the author.

Acknowledgements

This work is in part supported by the National Science Foundation (ECCS-0846502 and ECCS-1307831) and the University of California Proof of Concept Program (POC-269200) to TP. RL and BN acknowledge the fellowship support from China Scholarship Council (CSC). Authors would also like to thank Yijun Zhang for his assistance on the device illustrations.

Received: May 12, 2014
Revised: June 17, 2014

---

[1] M. L. Hammock, A. Chortos, B. C. Tee, J. B. Tok, Z. Bao, *Adv. Mater.* **2013**, *25* 5997.
[2] A. V. Shirinov, W. K. Schomburg, *Sens. Actuat. A: Phys.* **2008**, *142*, 48.
[3] L. Chunyan, P. Wu, L. Soohyun, A. Gorton, M. J. Schulz, C. H. Ahn, *J. Microelectromech. Syst.* **2008**, *17*, 334.
[4] M. S. Kim, S. E. Jo, D. H. Kang, H. R. Ahn, Y. J. Kim, presented at *17th Int. Conf. Solid-State Sensors, Actuators and Microsystems (Transducers and Eurosensors XXVII)*, Barcelona, Spain, January **2013**.
[5] T. Someya, T. Sekitani, S. Iba, Y. Kato, H. Kawaguchi, T. Sakurai, *Proc. Natl. Acad. Sci. USA* **2004**, *101*, 9966.
[6] K. Takei, T. Takahashi, J. C. Ho, H. Ko, A. G. Gillies, P. W. Leu, R. S. Fearing, A. Javey, *Nat. Mater.* **2010**, *9*, 821.
[7] T. Sekitani, Y. Noguchi, K. Hata, T. Fukushima, T. Aida, T. Someya, *Science* **2008**, *321*, 1468.
[8] K. F. Lei, K. Lee, M. Lee, *Microelectron Eng* **2012**, *99*, 1.
[9] W. Chang, T. Fang, S. Yeh, Y. Lin, *Sensors* **2009**, *9*, 1188.
[10] G. Schwartz, B. C. Tee, J. Mei, A. L. Appleton, D. H. Kim, H. Wang, Z. Bao, *Nat. Commun.* **2013**, *4*, 1859.
[11] Y. Hotta, Y. Zhang, N. Miki, *Micromachines* **2012**, *3*, 137.
[12] C. C. Chiang, C. Lin, M. S. Ju, *Sens. Actuat. A: Phys.* **2007**, *134*, 382.
[13] D. J. Lipomi, M. Vosgueritchian, B. C. Tee, S. L. Hellstrom, J. A. Lee, C. H. Fox, Z. Bao, *Nat. Nanotechnol.* **2011**, *6*, 788.
[14] A. Levi, M. Piovanelli, S. Furlan, B. Mazzolai, L. Beccai, *Sensors* **2013**, *13*, 6578.
[15] M. Ramuz, B. C. Tee, J. B. Tok, Z. Bao, *Adv. Mater.* **2012**, *24*, 3223.
[16] M. S. White, M. Kaltenbrunner, E. D. Glowacki, K. Gutnichenko, G. Kettlgruber, I. Graz, S. Aazou, C. Ulbricht, D. Egbe, M. C. Miron, Z. Major, M. C. Scharber, T. Sekitani, T. Someya, S. Bauer, N. S. Sariciftci, *Nat. Photon.* **2013**, *7*, 811.
[17] J. Viventi, D. H. Kim, L. Vigeland, E. S. Frechette, J. A. Blanco, Y. S. Kim, A. E. Avrin, V. R. Tiruvadi, S. W. Hwang, A. C. Vanleer, D. F. Wulsin, K. Davis, C. E. Gelber, L. Palmer, J. Van der Spiegel, J. Wu, J. L. Xiao, Y. G. Huang, D. Contreras, J. A. Rogers, B. Litt, *Nat. Neurosci.* **2011**, *14*, 1138.
[18] R. D. Ponce Wong, J. D. Posner, V. J. Santos, *Sens. Actuat. A: Phys.* **2012**, *179*, 62.
[19] P. Yong-Lae, C. Bor-Rong, R. J. Wood, *IEEE Sens. J.* **2012**, *12*, 2711.
[20] C. Y. Wu, W. H. Liao, Y. C. Tung, *Lab Chip* **2011**, *11*, 1740.
[21] M. C. Liu, H. C. Shih, J. G. Wu, T. W. Weng, C. Y. Wu, J. C. Lu, Y. C. Tung, *Lab Chip* **2013**, *13*, 1743.
[22] Y. L. Park, C. Majidi, R. Kramer, P. Berard, R. J. Wood, *J. Micromech. Microeng.* **2010**, *20*, 125029.
[23] J. B. Chossat, P. Yong-Lae, R. J. Wood, V. Duchaine, *IEEE. Sens. J.* **2013**, *13*, 3405.
[24] K. Chung, H. Lee, H. Lu, *Lab Chip* **2009**, *9*, 3345.
[25] S. Zhao, H. Cong, T. Pan, *Lab Chip* **2009**, *9*, 1128.
[26] Y. Ding, L. Hong, B. Nie, K. S. Lam, T. Pan, *Lab Chip* **2011**, *11*, 1464.
[27] B. Nie, R. Li, J. D. Brandt, T. Pan, *Lab Chip* **2014**.
[28] R. O. G. L. Barrett, *Information Display Magazine* **2010**, *3*, 16.
[29] L. Pan, A. Chortos, G. Yu, Y. Wang, S. Isaacson, R. Allen, Y. Shi, R. Dauskardt, Z. Bao, *Nature Commun.* **2014**, *5*, 3002.
[30] W. C. O'Mara, *Liquid Crystal Flat Panel Displays: Manufacturing Science and Technology*, Van Nostrand Reinhold, New York **1993**.
[31] E. Lueder, *Liquid Crystal Displays* Ed. 4, John Wiley and Sons Ltd, Chichester, UK, **2010**.
[32] A. K. Bhowmik, Z. Li, P. J. Bos, *Mobile Displays: Technology and Applications*, John Wiley and Sons Ltd, Chichester, UK, **2008**.
[33] W. Den Boer, *Active Matrix Liquid Crystal Displays: Fundamentals and Applications*, Elsevier, Burlington, MA, USA, **2005**.
[34] T. Pan, W. Wei, *Ann. Biomed. Eng.39*, **2010**, 600.
[35] W. Y. Tseng, J. S. Fisher, J. L. Prieto, K. Rinaldi, G. Alapati, A. P. Lee, *J. Micromech. Microeng.* **2009**, *19*, 085002.
[36] M. Di Giovanni, *Flat and Corrugated Diaphram Design Handbook*-Marcel Dekker, New York **1982**.
[37] E. Vassent, G. Meunier, A. Foggia, G. Reyne, *IEEE T. Magn.* **1991**, *27*, 5232.
[38] X. Lai, D. A. Liu, L. Peng, J. Ni, *J. Power Sources* **2008**, *182*, 153.
[39] J. O. P. A. Bastos, *Electromagnetic Modeling by Finite Element Methods*, Marcel Dekker, New York **2003**.
[40] C. A. Neugebauer, M. B. Webb, *J Appl Phys* **1962**, *33*, 74.
[41] M. C. Potter, D. C. Wiggert, B. H. Ramadan, *Mechanics of Fluids SI Version*, Cengage Learning, Independence, KY, USA, **2011**.
[42] W. M. Haynes, D. R. Lide, T. J. Bruno, *CRC Handbook of Chemistry and Physics 2012–2013*, CRC Press, Boca Raton, FL, USA, **2012**.
[43] G. P. Association, *Physical Properties of Glycerine and its Solutions*-Glycerine Producers' Association, New York, **1963**.
[44] H. B. Zhang, M. J. Edirisinghe, S. N. Jayasinghe, *J. Fluid Mech.* **2006**, *558*, 103.
[45] Dow Chemical Company, http://msdssearch.dow.com/PublishedLiteratureDOWCOM/dh_0037/0901b80380037a64.pdf?filepath=propyleneglycol/pdfs/noreg/117-01540.pdf&fromPage=GetDoc (accessed: August 2014).
[46] MEGlobal,http://www.meglobal.biz/media/product_guides/MEGlobal_MEG.pdf (accessed: August 2014).
[47] J. S. Lewis, M. S. Weaver, *IEEE J. Sel. Top Quant.* **2004**, *10*, 45.
[48] S. Bae, H. Kim, Y. Lee, X. Xu, J. Park, Y. Zheng, J. Balakrishnan, T. Lei, H. R. Kim, Y. I. Song, Y. Kim, K. S. Kim, B. Ozyilmaz, J. Ahn, B. H. Hong, S. Iijima, *Nat. Nanotechnol.* **2010**, *5*, 574.
[49] H. Yamaguchi, *Engineering Fluid Mechanics* Vol. *85*, Springer, Dordrecht, Netherlands, **2008**.
[50] C. Pang, G. Y. Lee, T. I. Kim, S. M. Kim, H. N. Kim, S. H. Ahn, K. Y. Suh, *Nat. Mater.* **2012**, *11*, 795.
[51] J. B. Mark, *Atlas of Cardiovascular Monitoring*, Churchill Livingstone, New York **1998**.
[52] K. Kohara, Y. Tabara, A. Oshiumi, Y. Miyawaki, T. Kobayashi, T. Miki, *Am. J. Hypertens.* **2005**, *18S*, 11S.
[53] S. Wållberg-Jonsson, K. Caidahl, N. Klintland, G. Nyberg, S. Rantapää-Dahlqvist, *Scand. J. Rheumatol.* **2008**, *37*, 1.
[54] N. R. Gaddum, J. Alastruey, P. Beerbaum, P. Chowienczyk, T. Schaeffter, *Ann. Biomed. Eng.* **2013**, *41*, 2617.
[55] Y. Z. Ding, S. Garland, M. Howland, A. Revzin, T. R. Pan, *Adv. Mater.* **2011**, *23*, 5551.